Resources, Conservation & Recycling 190 (2023) 106812

Contents lists available at ScienceDirect

Resources, Conservation & Recycling

journal homepage: www.elsevier.com/locate/resconrec

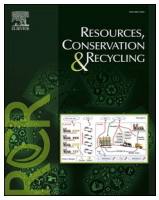

Full length article

Modeling the mechanical properties of recycled aggregate concrete using hybrid machine learning algorithms

Yiming Peng, Cise Unluer *

School of Engineering, University of Glasgow, Glasgow G12 8LT, United Kingdom

ARTICLE INFO

Keywords:
Recycled aggregate concrete
Compressive strength
Artificial neural network
Support vector machine
Hybrid models
Partial dependence plot
Shapley additional explanations

ABSTRACT

To explore the complicated functional relationship between key parameters such as the recycled aggregate properties, mix proportion and compressive strength of recycled aggregate concrete (RAC), a complete database involving 607 records from relevant published literature was built. Two standard algorithms (artificial neural network (ANN) and support vector regression (SVR)) and two optimized hybrid models (Particle Swarm Optimization based SVR (PSO-SVR) and grey Wolf optimizer based SVR (GWO-SVR)) were adopted. Furthermore, two interpretable algorithms (Partial Dependence Plot (PDP) and SHapley Additive exPlanations (SHAP)) were utilized to assess the global and local approaches independent of machine learning models, contributing towards decision-making rationales. Results indicated that the coefficient of determination (R^2) of ANN, SVR, PSO-SVR and GWO-SVR were 0.7569, 0.5914, 0.8995 and 0.9056 respectively, showing that hybrid models outperformed the conventional models. However, GWO-SVR was the most problematic with overfitting when analyzing its three subsets. The two feature importance analyses revealed cement content, water content, natural fine aggregates, and water absorption as significant characteristics that affect mechanical performance.

1. Introduction

Reduction of carbon dioxide (CO_2) emissions associated with key industries such as building and construction plays a crucial role in achieving climate neutrality by 2050 (Rosa et al., 2022). Among these, the use of building materials, a major one of which is concrete, is a significant source of CO_2 emissions. The annual production of >4 billion metric tons of Portland cement on a global basis accounts for 8–10% of global anthropogenic CO_2 emissions (Her et al., 2021; Poudyal and Adhikari, 2021). Construction and demolition waste, one of the main by-products of fast industrialization and urbanization, involves various solid wastes generated in the construction of new buildings, and the reconstruction and demolition of older or unwanted structures. These include leftover concrete blocks, waste mortars, and waste bricks, with a trace of steel, wood, and decorative materials thrown in for good measure (Ma et al., 2022; Nunes and Mahler, 2020; Wang et al., 2021). Consumption of natural resources and the inability to properly dispose of building waste is undoubtedly a significant impediment to sustainable development. Recycling and reusing construction waste are critical in achieving a sustainable built environment, both in terms of environmental protection and resource efficiency (Habibi et al., 2021). In terms of resource management, identification of the key factors that control the mechanical properties of recycled building components can facilitate the reuse of these products on a larger scale than currently practiced, thereby enabling the conservation of natural resources and recycling of these materials in value added applications rather than contributing to landfill.

Recycled aggregate concrete (RAC) involves recycled concrete aggregates obtained after crushing, cleaning, and grading of waste concrete blocks, which either partially or completely replace natural sand and gravel (Guo et al., 2018; Shi et al., 2016; Tam et al., 2021). The primary distinction between recycled aggregates and natural aggregates is that the former is composed of internal natural aggregates and external surfaces covered by hardened mortar. The porous structure of the hardened mortar on the surface of the recycled aggregates results in a high porosity, high water absorption, and low density (Kwan et al., 2012; Tam et al., 2020). Additionally, recycled aggregates have larger interfacial transition zones (ITZ) than their natural counterparts due to the presence of older ITZ in the recycled aggregate, in addition to the new ITZ that forms during the hardening process (Kazmi et al., 2021; Xiao et al., 2013). Excessive recycled aggregate contents have been demonstrated to increase the porosity of concrete and reduce the bond

* Corresponding author.
E-mail address: Cise.Unluer@glasgow.ac.uk (C. Unluer).

https://doi.org/10.1016/j.resconrec.2022.106812
Received 6 July 2022; Received in revised form 4 November 2022; Accepted 29 November 2022
Available online 11 December 2022

Table 1
Distribution properties of input and output parameters.

Classification	Variable	Unit	Category	Statistics			
				Min	Max	Average	STDEV
Recycled aggregate properties	Density	kg/m^3	Input	2000	2681	2414.09	121.43
	Water absorption	%	Input	0.886	12.7	4.98	1.87
Mixture Proportions	Water content	kg/m^3	Input	73	290	182.68	29.70
	Cement	kg/m^3	Input	225	864	410.92	94.06
	Natural fine aggregates	kg/m^3	Input	0	1317	712.78	197.07
	Recycled coarse aggregates	kg/m^3	Input	0	1731	592.24	377.20
	Natural coarse aggregates	kg/m^3	Input	0	1614	404.01	391.40
	Superplasticizer	kg/m^3	Input	0	222.6	4.06	18.60
Mechanical property	Compressive strength	MPa	Output	6.06	104.1	40.80	14.82

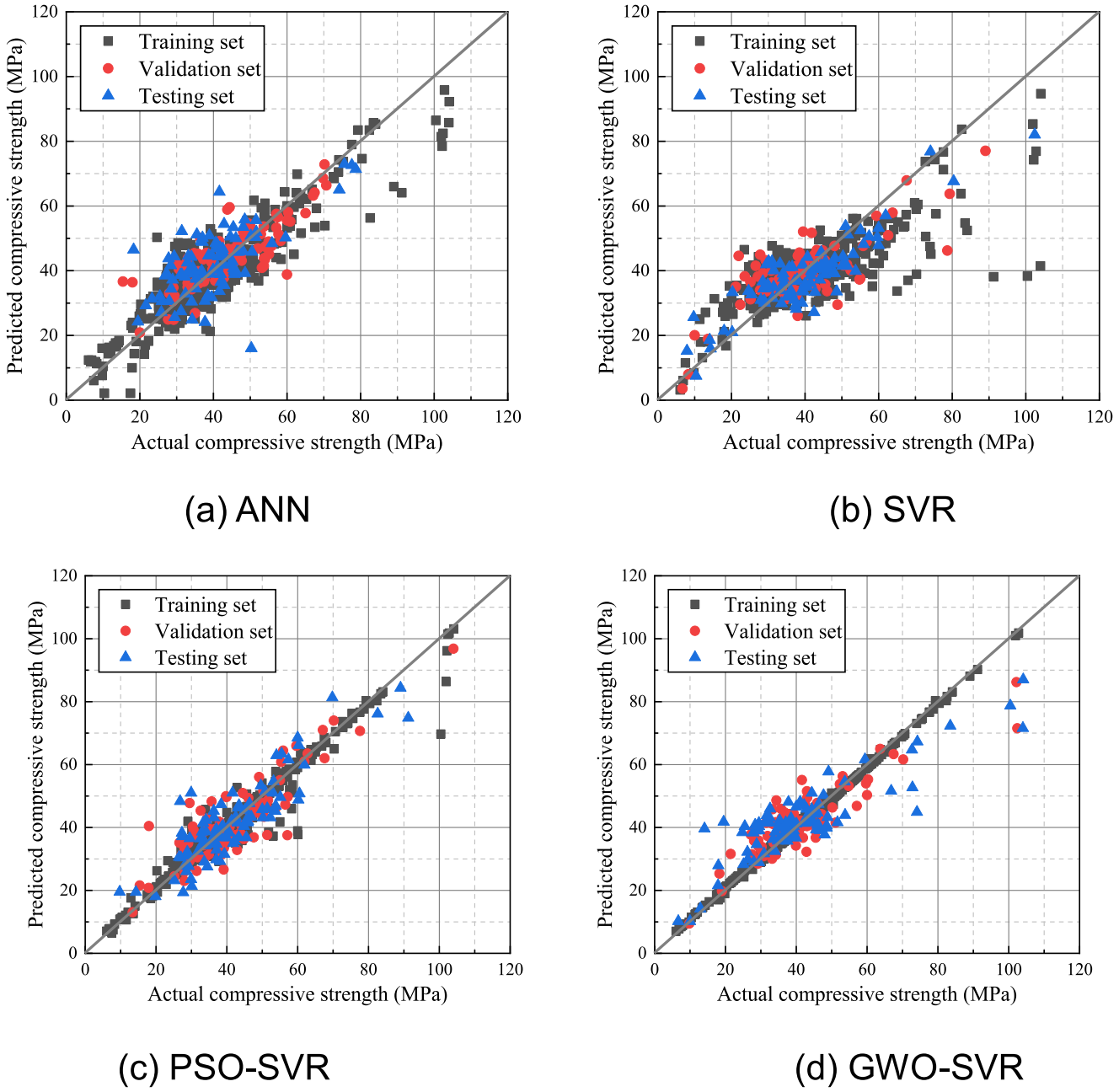

Fig. 1. Correlation between the actual and predicted compressive strength of recycled aggregate concrete. (a) ANN (b) SVR (c) PSO-SVR (d) GWO-SVR.

Table 2
Statistical indicator results of different machine learning models.

		R^2	RMSE	MAE	MAPE	RSR
ANN	Training	0.8121	6.822	5.141	14.63	0.4334
	Validation	0.6381	7.212	5.575	14.82	0.6016
	Testing	0.3590	9.005	6.968	19.58	0.8006
	All	0.7569	7.301	5.479	15.62	0.4931
SVR	Training	0.5581	9.951	6.848	17.41	0.6648
	Validation	0.5986	8.601	6.534	18.84	0.6335
	Testing	0.7464	7.214	6.034	17.84	0.5036
	All	0.5914	9.464	6.679	17.95	0.6392
PSO- SVR	Training	0.9476	3.451	1.859	4.808	0.2289
	Validation	0.7573	6.761	5.310	14.11	0.4927
	Testing	0.7689	6.609	5.245	14.21	0.4808
	All	0.8995	4.693	2.884	7.715	0.3170
GWO- SVR	Training	0.9954	0.971	0.945	2.678	0.0681
	Validation	0.7508	6.794	4.987	12.64	0.4992
	Testing	0.7193	9.270	6.613	18.38	0.5298
	All	0.9056	4.549	2.401	6.608	0.3072

strength in the ITZ, resulting in decreased compressive and tensile strengths, and elastic modulus (Kwan et al., 2012). These adverse effects can be alleviated by various pretreatment methods applied to these aggregates to enhance their performance.

As with ordinary concrete, the mechanical properties of RAC are affected by curing conditions (Gayarre et al., 2014), mineral admixtures (Kou et al., 2011a), chemical admixtures (Kannan et al., 2021) and aggregate properties (Ozbakkaloglu et al., 2018). In addition to the investigation of the mechanisms by which raw material properties and mix proportion affect the strength of RAC, there is a focus on the development of mathematical functions or models to predict the mechanical properties and constitutive equations (stress-strain curve expression) under uniaxial stress state (Guo et al., 2019; Liang et al., 2017; Peng et al., 2019). However, these mathematical expressions are often hampered by their inability to attain high forecast accuracy due to a lack of sufficient fitting parameters. They are constrained to a certain kind of function expression throughout the prediction process, in contrast to RAC's high degree of flexibility. As a result, the proposed functions generally fail to properly predict RAC performance.

Machine learning (ML), including both supervised and unsupervised learning, is increasingly regarded as a formidable contender to classic linear or nonlinear regression methods for predicting the mechanical strength of RAC. Using ML instead of conventional empirical or semi-empirical models enables better adaptation to diverse databases since function expressions are not rigidly enforced (Peng and Unluer, 2022). In addition, in the presence of several influencing factors, the conventional techniques are plainly insufficient. This is because when an influencing factor is included, the function expression is seldom as straightforward as just adding an independent variable to the original basis, which is not an issue for ML. Among the several ML models available, artificial neural network (ANN) and support vector machine (SVM) are the two well-known and frequently used techniques (Deng et al., 2021; Yan and Shi, 2010; Yeh, 1998). ANN is a massively parallel interconnected network composed of adaptive simple units. Its organizational structure can simulate the interactive response of the biological nervous system to real-world objects. SVM, which evolved from binary data categorization, is a statistically-based ML technique for data optimization. In addition to these traditional algorithms, some recently developed algorithms are also used to optimize the hyperparameters of these traditional algorithms, such as genetic algorithm (Yuan et al., 2014), particle swarm optimization (PSO) algorithm (Qi et al., 2018) and grey wolf optimizer (GWO) (Behnood and Golafshani, 2018). The implementation of these hybrid algorithms is more conducive to the rational selection of the optimal ML model for various datasets.

The overall aim of this work is to present an applied model and analysis of the relationship between the key factors and outcomes to facilitate the optimization of the use of RAC in the built environment. To evaluate the complicated functional relationship between key parameters such as the recycled aggregate properties, mix proportion and compressive strength of RAC, an extensive dataset accessible in published literature was developed in this study. On this basis, four machine learning models, including two traditional models (ANN and support vector regression (SVR)) and two hybrid models (PSO based SVR and GWO based SVR) were used to predict the compressive strength of RAC, and their calculation results were compared by different performance evaluation methods. However, considering the non-visual characteristics of ML, in order to clearly analyze how the initial variables affect the final results, partial dependence plot (PDP) and Shapley Additive exPlanations (SHAP) were used. This enabled the evaluation of the relationship between a feature and the expected responses for each observation, comparison of the importance of predictor variables, and investigation of the joint influence of the two variables on the prediction results.

2. Materials and methodology

2.1. Machine learning model development

ANN is a mathematical model formed by imitating the structure and function of a biological system (Fig. A1(a)) (Zhang et al., 2021). As a result, it has many of the properties of biological brain systems, including (i) adaptation and self-study, (ii) computational parallelism and storage distribution, (iii) nonlinear mapping, and (iv) robustness/-fault tolerance (Chen et al., 1995). The powerful nonlinear processing capability of artificial neural networks fuels researchers' enthusiasm for the technology on a daily basis. Among them, the backpropagation neural network is the most mature and widely used multilayer feed-forward network structure. In terms of learning rules, it is also a supervised learning network because it can change its own structure and weights between neurons through continuous learning of sample data without knowing in advance that there is a specific mapping relationship between network input and output, and finally realize the correct mapping.

In general, SVM turns the input space into a high-dimensional space through a nonlinear transformation defined by the inner product function and then determines the generalized optimal classification surface in this space. Most linear non-separable issues in input space can be turned into linear separable problems in feature space using the proper mapping function. SVM is primarily utilized in classification and regression, with SVR often employed to tackle prediction and regression-related issues (Fig. A1(b)) (Saha et al., 2020).

Along with the two relatively classic single ML algorithms mentioned above, various enhanced hybrid algorithms have been created for hyperparameter optimization of traditional methods. PSO and GWO are two examples of standard optimization methods. PSO and GWO are both examples of bionic algorithms. The former is derived from simulation studies on bird foraging behavior, while the latter is derived from wolves' hierarchy and predation strategy simulations (Behnood and Golafshani, 2018; Qi et al., 2018). To optimize and acquire the ideal solution for the goal, PSO utilizes a process of information exchange. It is an algorithm for population-based intelligent optimization. PSO has been extensively employed due to its small number of parameters, straightforward procedure, and, most significantly, its success in multiclass optimization situations. In comparison to other heuristic algorithms, GWO offers the following advantages: simplicity of design, few parameters, ease of modification, rapid convergence speed, and powerful local search capability.

2.2. Concrete database collection

Proper data sets must be organized prior to performing ML computations. Not only should an acceptable data collection comprise a high number of samples (i.e. the bigger the sample set, the more extensively

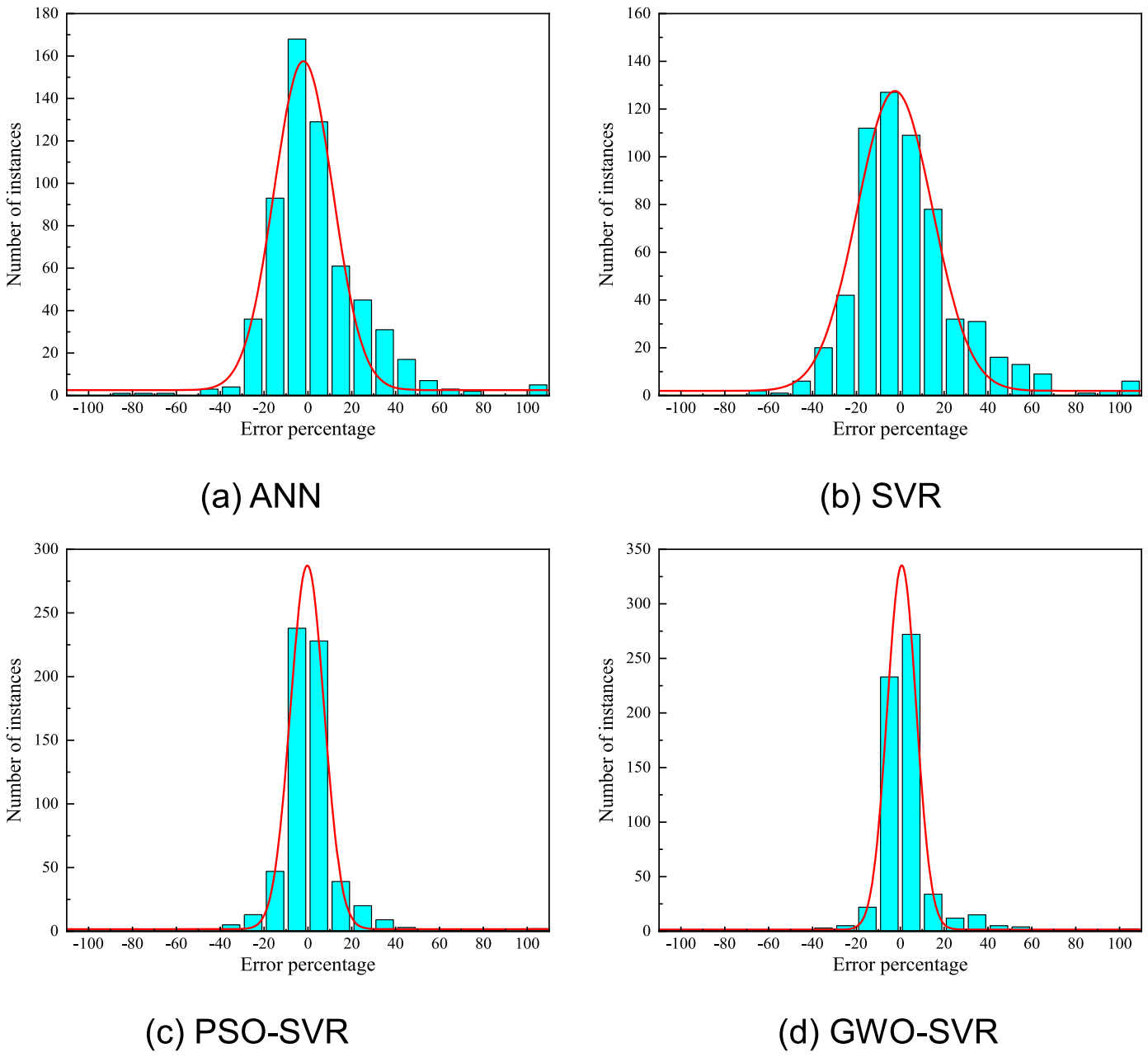

Fig. 2. Error percentage distribution histogram. (a) ANN (b) SVR (c) PSO-SVR (d) GWO-SVR.

and deeply the ML model can investigate the possible association between variables), but should also contain all factors that can impact the findings. Only after achieving the preceding two criteria can the proposed problem be adequately solved.

Following this approach, to widen the coverage of the collected data as much as possible, 607 experimental data sets were acquired from 87 publications (Abdulla, 2015; Adams et al., 2016; Anastasiou et al., 2018; Bai et al., 2020; Belén et al., 2011; Beltrán et al., 2014; Bhagat et al., 2014; Butler et al., 2013, 2014; Çakır and Sofyanlı, 2015; Carneiro et al., 2014; Casuccio et al., 2008; Chen et al., 2021; Corinaldesi, 2010; Dhanya et al., 2020; Dilbas and Güneş, 2021; Dilbas et al., 2014; Domingo-Cabo et al., 2009; Du et al., 2021; Duan et al., 2020; Duan and Poon, 2014; Etxeberria et al., 2007a, 2007b; Fathifazl et al., 2011; Fiol et al., 2020; Folino and Xargay, 2014; Gao et al., 2019, 2015; García-González et al., 2015; Gayarre et al., 2014; Gökçe and Şimşek, 2013; Gómez-Soberón, 2002; Gomez et al., 2001; Gonzalez-Corominas and Etxeberria, 2016; González-Fonteboa and Martínez-Abella, 2008; González et al., 2021; Gunasekara et al., 2020; Gupta et al., 2020; Haitao and Shizhu, 2015; Huang et al., 2017; Ismail and Ramli, 2013; Juan-Valdes et al., 2021; Kim et al., 2013, 2016, 2015; Kim et al., 2019; Kou et al., 2011b, 2014; Li et al., 2021; Liang et al., 2021; Lin et al., 2004; Ling and Jiguang, 2018; Liu et al., 2021; Malešev et al., 2010; Manzi et al., 2013, 2017; Martinez et al., 2022; Medina et al., 2014; Mohammed et al., 2018; Nepomuceno et al., 2018; Nieto et al., 2019; Nili et al., 2019; Ozbakkaloglu et al., 2018; Pani et al., 2020; Pavlů et al., 2019; Pereira-de-Oliveira et al., 2014; Poon et al., 2007; Poon et al., 2004a; Poon et al., 2004b; Rangel et al., 2020; Santos et al., 2017; Savva et al., 2021; Setkit et al., 2021; Sharaky et al., 2021; Sheen et al., 2013; Silva et al., 2021; Soares et al., 2014; Somna et al., 2012; Sriravindrarajah et al., 2012; Taffese, 2018; Tam et al., 2015; Tang et al., 2016; Thomas et al., 2018; Ulloa et al., 2013; Yang et al., 2008; Yang, 2018; Younis and Pilakoutas, 2013).

The distribution properties of input and output parameters are listed in Table 1. In addition to the mix proportion, the properties of recycled

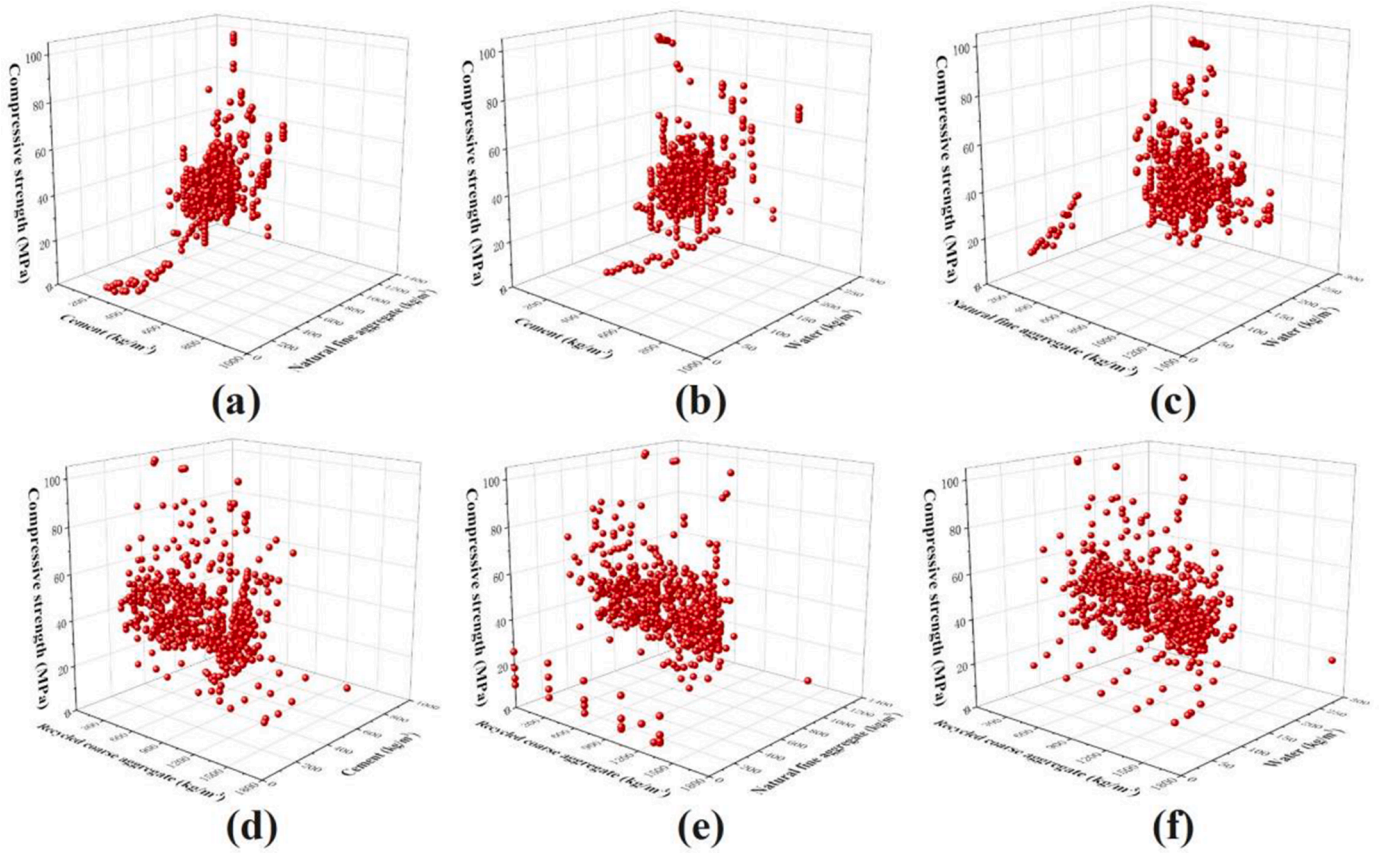

Fig. 3. 3D plots showing the 28-day compressive strength of RAC in relation to the (a) cement content and natural fine aggregates, (b) cement content and water content, (c) natural fine aggregates and water content, (d) recycled coarse aggregates and cement content, (e) recycled coarse aggregates and natural fine aggregates, and (f) recycled coarse aggregates and water content.

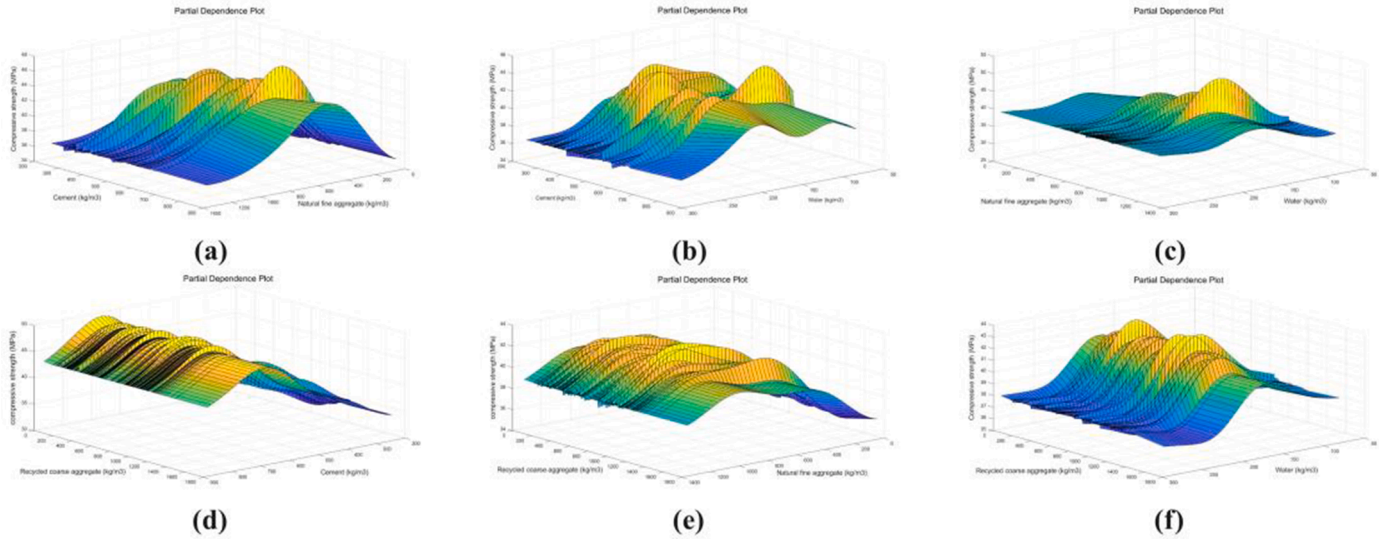

Fig. 4. Visualization of predicted responses using PDP.

aggregates also have a considerable effect on the ultimate strength of RAC systems. Therefore, all input variables of this study were screened for these two aspects. For recycled aggregates, the primary properties to consider were set as particle size distribution/fineness modulus, density, water absorption, and LA abrasion. For the mix proportion, the contents of recycled coarse (fine) aggregates, water, cementitious materials (including cement and other mineral admixtures), natural coarse (fine) aggregates, and chemical admixtures were taken into account. It should be noted that some parameters were difficult to obtain using the unified test techniques described in the preceding references (e.g. some sources provide the fineness modulus of aggregates, whereas others illustrate the percentage distribution of aggregates in each particle size range, or only indicate a very rough particle size range such as the maximum and minimum particle sizes). Following further screening, eight parameters

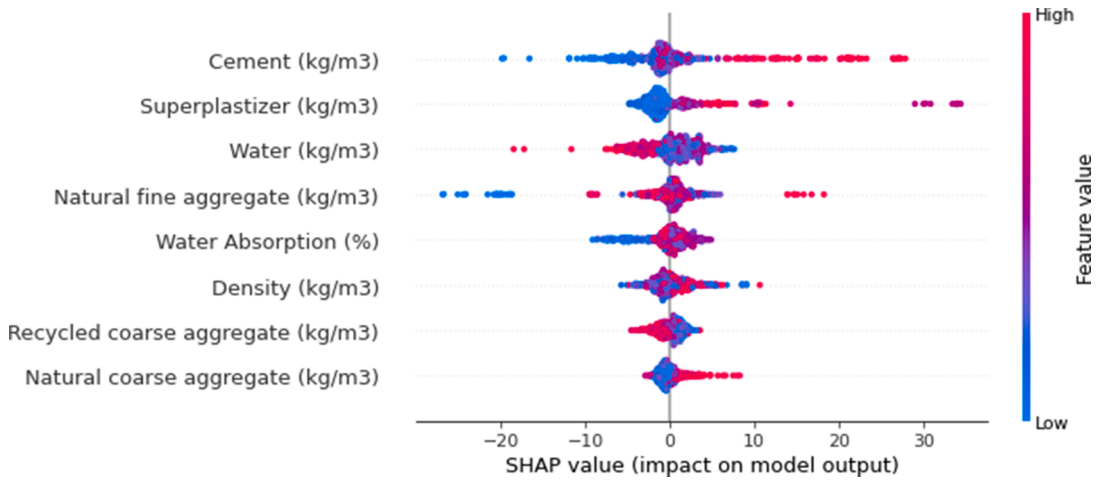

Fig. 5. Summary of the SHAP analysis showing the influence of eight parameters.

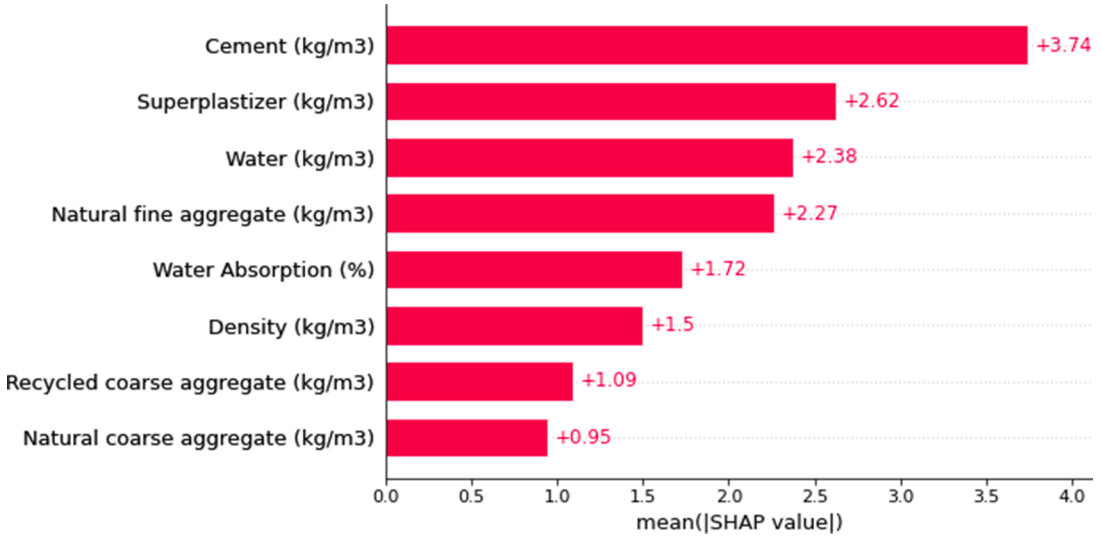

Fig. 6. Mean absolute value of the SHAP values for each feature.

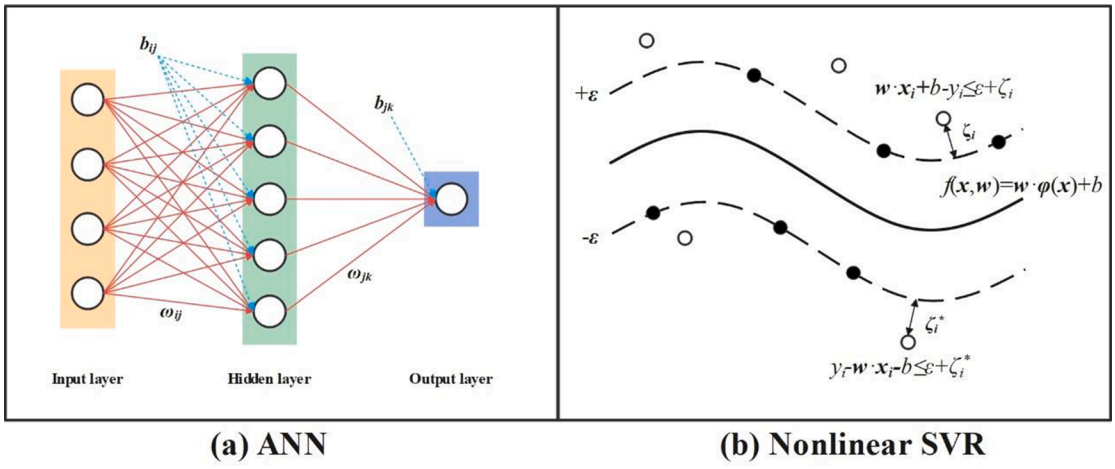

Fig. A1. Schematic diagrams of two typical machine learning algorithms (ANN and nonlinear SVR), adapted from (Asteris et al., 2021; Saha et al., 2020).

were chosen for ML calculation, two of which were recycled aggregate parameters, and the other six belonged to mix design parameters, including: (i) density of recycled aggregates (kg/m^3), (ii) water absorption of recycled aggregates (%), (iii) water content (kg/m^3), (iv) cement content (kg/m^3), (v) natural fine aggregate content (kg/m^3), (vi) recycled coarse aggregates content (kg/m^3), (vii) natural coarse

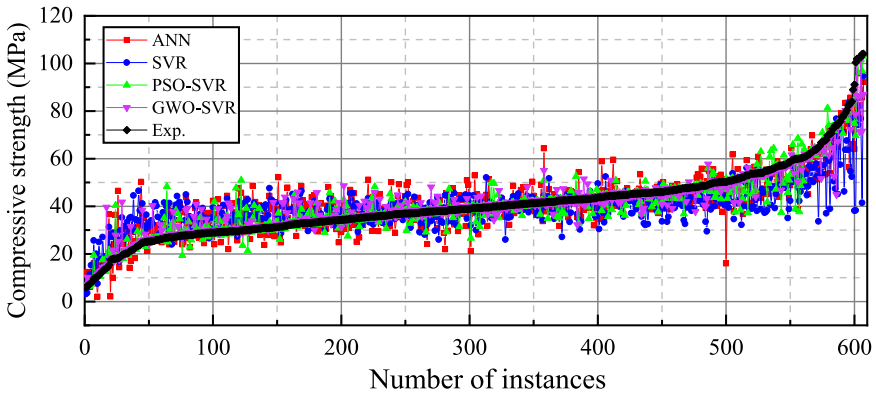

Fig. A2. Results calculated by different ML algorithms according to the ascending order of experimental value.

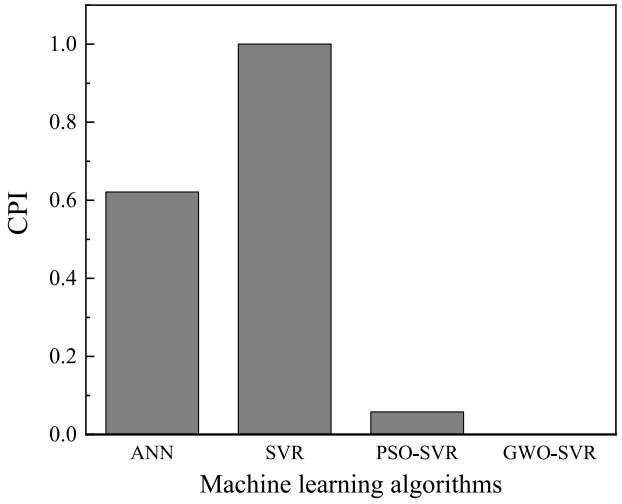

Fig. A3. CPI values based on different machine learning algorithms.

aggregates content (kg/m^3), and (viii) superplasticizer content (kg/m^3).

2.3. Performance assessment

The experimental database was often randomly separated into three subsets based on the categorization of the majority of prior studies: the training set, the validation set, and the testing sets (Chaabene et al., 2020). The training set was used to train the model's parameters (for example, in the case of an ANN, this is the process of continually optimizing the weight and bias); the validation set was used to assess the model's state and convergence throughout the training process. It was often used to alter the hyperparameters; the testing set was used to assess the model's generalizability, or the capacity of the model to effectively forecast a given set of new databases after optimizing the hyperparameters.

Four ML models were compared based on absolute error, error percentage, coefficient of determination (R^2), root mean squared error (*RMSE*), mean absolute percentage error (*MAPE*), mean absolute error (*MAE*), and *RMSE*-to-observation's standard deviation ratio (*RSR*) in order to assess the prediction performance difference Asteris et al., 2021). The closeness of the anticipated value to the actual value could be quantified using these techniques. The assessment of a single sample (mix proportion) accounted for the first two parameters, while the algorithm fitting degree of several subsets accounted for the last five. In addition, these five statistical parameters could also be set into a unified measurement parameter, namely the composite performance index (*CPI*) (Cook et al., 2019). The aforementioned eight parameters are expressed as Eqs. (1)-(8), where yi' and yi are the predicted value and actual value, respectively. $\bar{y}$ is the average value, P_j is the statistical parameter of the j-th parameter. $P_{min,j}$ and $P_{max,j}$ are the minimum and maximum values of the j^{th} statistical parameter across the five values using the same ML model.

$$Absolute\ error = y_i^{'} - y_i \tag{1}$$

$$Error\ percentage = \frac{y^{'}_i - y_i}{y_i} \tag{2}$$

$$R^2 = 1 - \frac{\sum_{i=1}^{n}(y^{'}_i - y_i)^2}{\sum_{i=1}^{n}(y_i - \bar{y})^2} \tag{3}$$

$$RMSE = \sqrt{\frac{\sum_{i=1}^{n}(y^{'}_i - y_i)^2}{n}} \tag{4}$$

$$MAE = \frac{1}{n}\sum_{i=1}^{n}|y^{'}_i - y_i| \tag{5}$$

$$MAPE = \frac{1}{n}\sum_{i=1}^{n}\left|\frac{y^{'}_i - y_i}{y_i}\right| \times 100 \tag{6}$$

$$RSR = \frac{RMSE}{\sqrt{\frac{1}{n}\sum_{i=1}^{n}(y_i - \bar{y})^2}} \tag{7}$$

$$CPI = \frac{1}{N}\sum_{j=1}^{N}\frac{P_j - P_{min,j}}{P_{max,j} - P_{min,j}} \tag{8}$$

2.4. Partial dependence plots (PDP)

The objective of a machine learning business application is to output judgments for decision-making. Model interpretability relates to a comprehension of the model's underlying process and output. The more interpretable a ML model is, the simpler it is for humans to comprehend why it makes certain conclusions or predictions. Its significance is reflected in the following: in the modeling stage, assist developers in comprehending the model, comparing and selecting the model, and optimizing and adjusting the model as necessary; in the operation stage, explain the model's internal mechanism to the business party and explain the model results. Whether learning the underlying connection of data or calculating or deriving the anticipated value, ML is commonly recognized as a black box operation, which necessitates the development of some interpretable local or global techniques for visually analyzing the ML process. Partial dependence plot (PDP) is a typical global interpretable technique. It is capable of not only representing the marginal influence of one or two features on the model's prediction

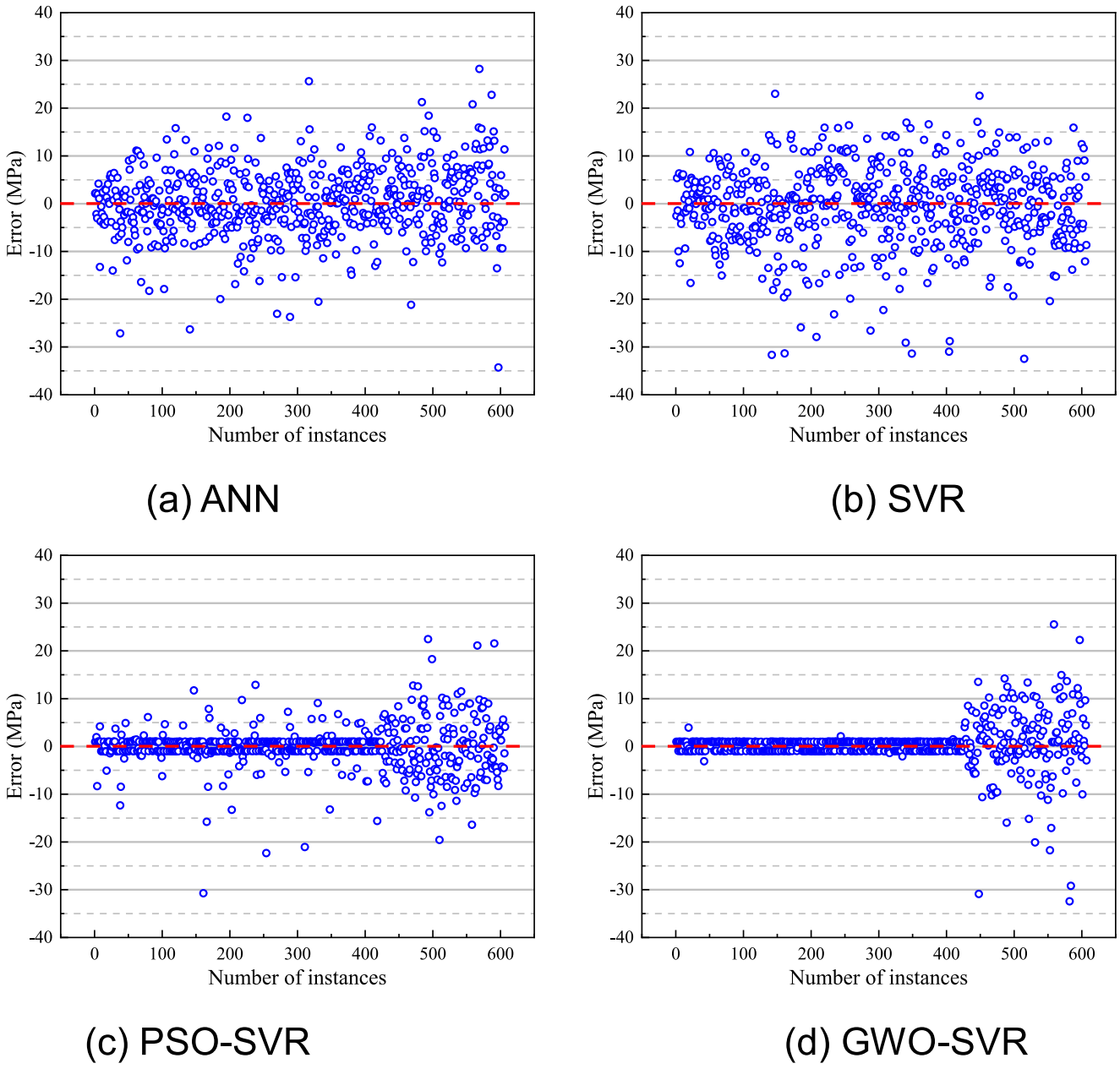

Fig. A4. Relative errors between actual and predicted compressive strength. (a) ANN (b) SVR (c) PSO-SVR (d) GWO-SVR.

outcomes, but also of ranking the relevance of features based on the operation results. PDP can show whether the relationship between target and feature is linear, monotonous, or more complicated (Friedman, 2001). The partial dependence function of regression is defined as follows:

$$\widehat{f}_{x_S}(x_S) = E_{x_C}\left[\widehat{f}_{x_S}(x_S, x_C)\right] = \int \widehat{f}_{x_S}(x_S, x_C) dP(x_C) \quad (9)$$

Where, x_S denotes the feature and the partial dependency function to be drawn, and x_C represents the other features that are used by the ML model $\widehat{f}$. Generally, set S has just one or two characteristics. The feature (s) in S that we are interested in are those that have an influence on the prediction. The combined feature vectors x_S and x_C define the whole feature space x. Partial dependency works by marginalizing the output of the ML model on the feature distribution in set C, resulting in a function that illustrates the link between the features in set C and the prediction outcomes. By marginalizing other features, a function that is dependent only on the features in S can be obtained, including their interaction.

2.5. Shapley additive exPlanations (SHAP)

The Shapley value is often used when discussing the distribution of interests in cooperative games. Its primary benefit is that its underlying principles and distribution outcomes are easily seen as equitable and acceptable by all stakeholders (Winter, 2002). The total inaccuracy of the combined prediction induced by the joint action of each individual prediction technique may be considered as income according to the use of Shapley value in income distribution. The income value can be allocated among several prediction techniques according to their "cooperative connection", i.e., the weight of each prediction method in the combined prediction model can be determined.

SHapley Additive exPlanations (SHAP) employs an additive feature attribution approach to generate an interpretable model, in which the output model is defined as the linear sum of the input variables. SHAP

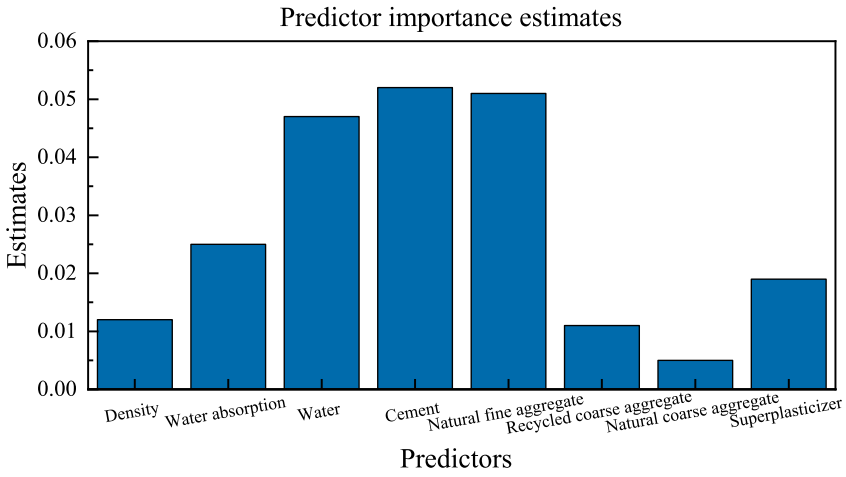

Fig. A5. Comparison of the importance of predictor variables.

Fig. A6. Local multiple force interpretation diagram based on XGBoost algorism (X_1: density, X_2: cement content, X_3: water content, X_4: water absorption, X_5: natural fine aggregates, X_6: recycled coarse aggregates, X_7: natural coarse aggregates, and X_8: superplasticizer).

defines the explanation as follows, where g corresponds to the model for explanation, M denotes the maximum size of the coalition and $z' \in \{0, 1\}^M$ represents whether the feature exists.

$$g(z') = \varphi_0 + \sum_{j=1}^{M} \varphi_j z_j' \tag{10}$$

The SHAP value of each feature represents the change predicted by the expected model under the condition of this input parameter. For each feature, the SHAP value indicates the contribution of the feature to the overall prediction results to illustrate the difference between the average model prediction and the actual prediction of the database. When $\varphi_i > 0$, it indicates that the feature can improve the predicted value; on the contrary, it indicates that the feature reduces the contribution.

3. Results and discussion

3.1. Performance assessments

In this study, the number of hidden layers of ANN is 1, with a total of 10 nodes, and the training algorithm is Levenberg-Marquardt (Lera and Pinzolas, 2002). Simultaneously, the radial basis function (RBF) is selected as the kernel function of the SVR algorithm (Blake and Kapetanios, 2003). For the hybrid algorithm, the maximum number of iterations of PSO and GWO is 100, in which the learning factors c_1 and c_2 of PSO are 1.5 and 1.7, respectively, and the particle swarm size is 20. Fig. 1 shows the comparison results between the predicted values and their respective actual values based on the selected four machine learning algorithms. Whichever model is chosen for prediction, the input data statistics in Table 2 reveal that the eight input variables have various dimensional units and orders of magnitude. Therefore, the parameter dimensions are normalized to remove their impact on the simulation outcomes prior to computation (Jo, 2019). In addition, the division proportion of the training set, validation set, and testing set is 70%, 15% and 15% (the corresponding number of data sets is 425, 91, and 91 respectively).

According to the prediction and analysis of the experimental data, it can be found that for the two traditional algorithms (ANN and SVR), there are a small number of test points with large deviations from the centerline in all three subsets, which is more obvious for the calculation results of SVR. In contrast, PSO and GWO can learn more about the relationship between input and output variables after optimizing the hyperparameters of SVR, resulting in superior fitting results for the hybrid models. Different from the illustration in Fig. 1 (random arrangement of sample data), Fig. A2 shows the results obtained after arranging the test values from small to large, and each value corresponds to the predicted values of different machine learning models. By arranging and integrating the data sets, it can be found that when the experimental compressive strength of ANN and SVR is large, the deviation between the predicted value and the actual value is greater. Similar to Fig. 1, the blue scatters in Fig. A2 that corresponds to the SVR changes significantly as the actual compressive strength exceeds 50 MPa.

Table 2 summarizes the evaluation parameters for three subsets and the total dataset, as determined by Eqs. (3)–(7). Similar to the visual interpretation of the findings in Fig. 1, although the R^2 of ANN is 0.8121 in the training set, it declines dramatically when extended to the validation and testing sets, with the testing set having a fitting accuracy of just 0.3590. In all three sets, the SVR method is difficult to provide adequate prediction results. PSO-SVR and GWO-SVR, by contrast, have much greater evaluation parameters than the two aforementioned methods, both in terms of subset and total dataset. Fig. A3 shows the results obtained after integrating the above five evaluation indexes into one index, i.e., CPI. The order of the CPI values from low to high is GWO-SVR, PSO-SVR, ANN, and SVR; in other words, GWO-SVR still achieves the highest score and exhibits the greatest prediction performance after considering all subsets and evaluation indicators. However, it should still be noted here that the R^2 corresponding to the GWO-SVR training set is as high as 0.9954, while in the testing set, the value is reduced to 0.7193, showing a significant reduction. While this is not the lowest value among the four methods, it does indicate that when GWO is employed for optimization, overfitting may occur (Abdel-Basset et al., 2020).

Along with describing the three subsets of the original database, it is important to perform a statistical analysis on each sample of data. The

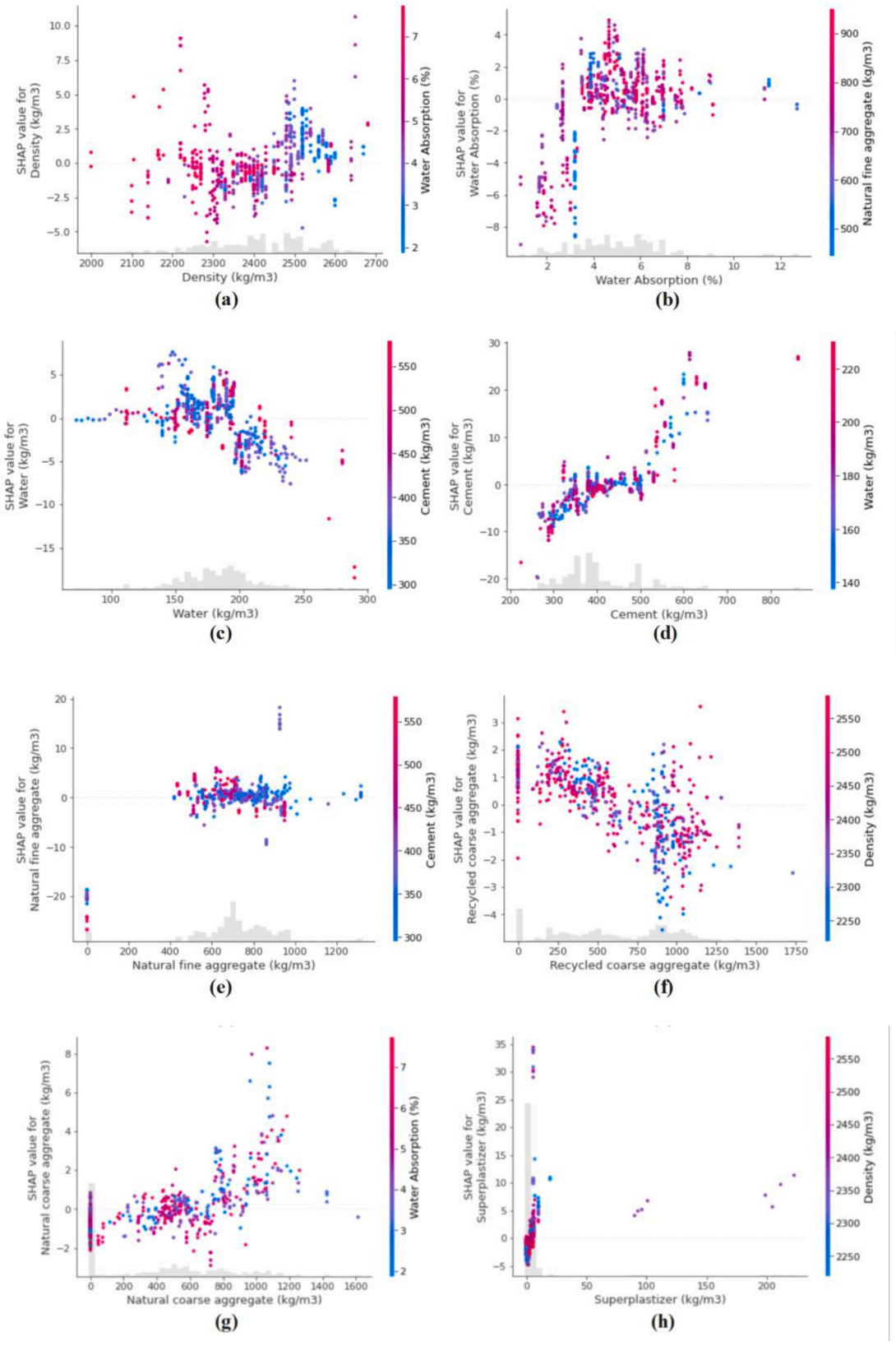

Fig. A7. Influence of single feature parameter on the SHAP value.

absolute error of each group of 607 samples in the total database is shown in Fig. A4. PSO-SVR and GWO-SVR exhibit the least degree of point dispersion in this regard. However, it is worth mentioning that the error value for the first 425 samples of GWO-SVR is really tiny, and then the error rapidly grows as the number of samples increases. This also verifies the earlier conjecture about the GWO-SVR algorithms, namely the phenomena of overlearning. Additionally, to account for the difference in absolute value across various mix proportions, the ratio of the

calculated absolute error to the actual value must be employed to quantify the degree of divergence of the forecast results from the true value. The histogram of the frequency distribution of the sample error percentage according to the statistics of various interval ranges is shown in Fig. 2. Clearly, when the error percentage of all samples acquired by an algorithm is closer to 0, this algorithm has a higher fitting accuracy. Although the number of samples with a GWO-SVR error percentage of −10%−10% is the highest in terms of frequency distribution, given that the majority of these samples are attributable to the training set's ultra-high fitting accuracy, the PSO-SVR method may exhibit more steady simulation capabilities by comparison.

3.2. PDP

Fig. A5 illustrates the calculation results performed using PDP to evaluate the significance of input variables. The concept of feature importance is critical in machine learning. It converts the effect of a feature on model prediction to a numerical value, which PDP can be used to depict the effect of this feature on prediction (Molnar et al., 2021). Unexpectedly, among the eight input variables, the three most important variables are cement, natural fine aggregate, and water content, but there is no input variable for recycled aggregate. Additionally, when the characteristics of recycled aggregate are further sorted, it is discovered that their density and water absorption have a greater effect on the predicted outcomes than their own content.

Alongside categorizing the input variables according to their feature importance, PDP makes an effort to visualize the machine learning operation process. In practice, feature sets often include just one or a maximum of two features, since only three-dimensional images can be used to define how input variables affect output variables. Fig. 3 is a 3D scatter diagram in which the upper three are drawn by selecting the top three predictors, i.e., water content, cement content, and natural fine aggregate, while the bottom three employ recycled coarse aggregate as the x-axis. The above variables are used respectively to investigate both the interaction of the three most significant variables and the influence of recycled aggregate content separately. As can be observed, there is no significant interacting connection between compressive strength and the selected variables, which may be owing to the low effect weights of two factors on the results induced by an excessive number of variables and a wide fluctuation range. In addition to the two coordinate axes shown in Fig. 3, there are six more factors that might have a substantial influence on the findings. Therefore, the link between PDP-based variables and output outcomes is reinforced to mitigate the effect of the other six elements. As shown in Fig. 4, the six surfaces are not as smooth as expected, indicating that even after minimizing the effect of other input factors, the chosen two variables still struggle to demonstrate a significant positive or negative relationship with compressive strength. Water content, cement content, and natural fine aggregate content all have a reasonable range, allowing the compressive strength to achieve its maximum value locally. When the recycled coarse aggregate content is used as the x-axis, regardless of which factor is used as the y-axis, the change of recycled coarse aggregate content is shown to not have a significant impact on the results.

3.3. SHAP

The contribution analysis of prediction outcomes based on Shapley value can be classified into two tiers according to the established model. On a global scale, the Shapley value distribution can be used to explain the unique effect, law, and correlation of characteristics; on a local scale, the quantitative contribution of each feature to each sample prediction can be specified (Liang et al., 2021). The typical contribution of each of the eight influencing parameters addressed in this investigation to the prediction outcomes, namely compressive strength, is shown in Fig. A6. The image depicts the viewpoint of a local interpretation. While it is likely that some of these features will have a positive influence on the outcomes (red bar area), others will have a negative impact (blue bar area). The visualization results shown in Fig. A6 indicate that recycled aggregate density, cement content, and natural and recycled coarse aggregate all have a beneficial effect on the outcomes within a particular range. On the contrary, water content has a detrimental effect on strength, while the force value of the X_8, i.e., superplasticizer, is 0, showing that it has no meaningful link with the final mechanical qualities. Additionally, the effect of each individual element on the outcome can be quantified, thus obtaining Fig. A7. It is readily apparent that the changing trend in RCA compressive strength with respect to these eight parameters is similar to that shown in the force diagram. For instance, in Fig. A7(c) and (d), the cement and water contents exhibit considerable positive and negative variations in response to the results. However, the change trend of several groups in Fig. A7 is different from Fig. A6, i.e., the change of scatter points (Fig. A7(b) and (f)) is in the opposite direction of the change depicted in the force diagram.

In contrast to local interpretation, global interpretation considers the cumulative effect of all distinct features on the results. As seen in Figs. 5 and 6, the first five significant features based on Shapley values are cement, superplasticizer, water content, natural fine aggregation, and water absorption. This ranking is comparable to the results of a PDP-based feature significance analysis, although there are still some discrepancies. Based on PDP findings, natural fine aggregate is regarded to be the second most significant influencing factor after cement content. This is reasonable since fine aggregate makes up a large proportion of the constituents in concrete to bind with the cement paste and larger aggregate to form strong connections. On the other hand, the effect weight of superplasticizer is rated second according to SHAP. However, Fig. A6 indicates that the content of superplasticizer does not correspond to either the positive or negative impact. This conflict may occur as a result of the asymmetric distribution of input parameters.

4. Conclusion

Reusing construction waste in RAC is an efficient and practical approach to achieve net-zero greenhouse gas emissions within building materials. This study aimed to use hybrid machine learning techniques (ANN, SVR, GWO-SVR and PSO-SVR) to reasonably predict the mechanical performance of RAC according to the given input parameters and present a solution for the inaccurate prediction abilities of traditional empirical models. Furthermore, two interpretable algorithms, PDP and SHAP, were used to reveal how variables specifically affected the compressive strength results. The performance of each model was evaluated, resulting in the following observations:

(1) For the two traditional machine learning models, ANN outperformed SVR in terms of prediction accuracy. The optimization algorithms were demonstrated to significantly improve the predictive ability of the SVR model. The evaluation of the eight statistical indicators in detail led to the identification of GWO-SVR as the most accurate model out of the four models, with an R^2 of 0.9056. PSO-SVR attained very similar results.
(2) The comparison and analysis of the actual and predicted values for each sample revealed very small errors for the first 425 groups of data in GWO-SVR. This outcome confirmed that hyperparameter optimization of SVR with GWO significantly improved its understanding of the training set. However, the training and testing phases exhibited large variations in results, especially with a deterioration in R^2 from 0.9954 to 0.7193 for GWO-SVR, indicating overfitting and leading to inaccuracies in the validating and testing phases. As a result, although GWO-SVR demonstrated a greater overall prediction accuracy than PSO-SVR, the latter may provide a more consistent prediction performance for the training, validation and testing sets.
(3) The PDP and SHAP algorithms were used to illustrate the principle of ML and to visualize its black-box operation process.

Although both feature importance and feature dependence analyses demonstrated that the two algorithms' output results were relatively similar, their ranking of feature significance remained distinct. While SHAP placed the influence weight of superplasticizer and water contents in front of natural fine aggregate content, PDP implied that the effect weight of natural fine aggregates content was second only to cement content. Furthermore, when compared to PDP, SHAP could demonstrate whether each input variable's impact on the output was positive or negative. In this respect, cement content, recycled aggregate density, and natural/recycled coarse aggregates contents all had a positive effect; whereas water content had a negative impact on the mechanical properties of RAC.

ML is regarded as a promising predictive tool for a wide range of engineering applications. With their continuous development, hybrid models reveal more accurate prediction performance than single algorithm models due to their hyperparameter optimization. Furthermore, global and local model-agnostic global interpretation techniques represented by PDP and SHAP provide algorithmic help for different users to understand the prediction basis behind the characteristics of ML black-box operations. The combination of these approaches can enable the accurate prediction of the mechanical performance of RAC based on existing data, thereby saving engineering costs, improving efficiency and enhancing the sustainability of building materials. For the widespread application of ML in the analysis of concrete materials, the further development of hyperparameter optimization algorithm (precursor algorithm) and the identification of the relevant experimental database are the focus of future research.

CRediT authorship contribution statement

Yiming Peng: Methodology, Investigation, Writing – original draft, Data curation. **Cise Unluer:** Resources, Writing – review & editing, Supervision, Project administration.

Declaration of Competing Interest

The authors declare that they have no known competing financial interests or personal relationships that could have appeared to influence the work reported in this paper.

Data availability

Data will be made available on request.

Acknowledgements

This work was funded by The Royal Society (project ref: ICA\R1 \201310) and China Scholarship Council (grant number: 202006370082).

Appendix

References

Abdel-Basset, M., El-Shahat, D., El-henawy, I., de Albuquerque, V.H.C., Mirjalili, S., 2020. A new fusion of grey wolf optimizer algorithm with a two-phase mutation for feature selection. Expert Syst. Appl. 139, 112824.
Abdulla, N.A., 2015. Effect of recycled coarse aggregate type on concrete. J. Mater. Civ. Eng. 27 (10), 04014273.
Adams, M.P., Fu, T., Cabrera, A.G., Morales, M., Ideker, J.H., Isgor, O.B., 2016. Cracking susceptibility of concrete made with coarse recycled concrete aggregates. Constr. Build. Mater. 102, 802–810.
Anastasiou, E., Papachristoforou, M., Anesiadis, D., Zafeiridis, K., Tsardaka, E.-.C., 2018. Investigation of the use of recycled concrete aggregates originating from a single ready-mix concrete plant. Appl. Sci. 8 (11), 2149.
Asteris, P.G., Skentou, A.D., Bardhan, A., Samui, P., Pilakoutas, K., 2021. Predicting concrete compressive strength using hybrid ensembling of surrogate machine learning models. Cem. Concr. Res. 145, 106449.
Bai, W., Li, W., Guan, J., Wang, J., Yuan, C., 2020. Research on the mechanical properties of recycled aggregate concrete under uniaxial compression based on the statistical damage model. Materials (Basel) 13 (17), 3765.
Behnood, A., Golafshani, E.M., 2018. Predicting the compressive strength of silica fume concrete using hybrid artificial neural network with multi-objective grey wolves. J. Clean. Prod. 202, 54–64.
Belén, G.-.F., Fernando, M.-.A., Diego, C.L., Sindy, S.-.P., 2011. Stress–strain relationship in axial compression for concrete using recycled saturated coarse aggregate. Constr. Build. Mater. 25 (5), 2335–2342.
Beltrán, M.G., Barbudo, A., Agrela, F., Galvín, A.P., Jiménez, J.R., 2014. Effect of cement addition on the properties of recycled concretes to reach control concretes strengths. J. Clean. Prod. 79, 124–133.
Bhagat, D.K., Parmer, J., Tank, Y.R., Gadhiya, D.H., 2014. Experimental study of compressive strength of recycled aggregate concrete. Int. J. Eng. Res. Technol. 3 (4).
Blake, A.P., Kapetanios, G., 2003. A radial basis function artificial neural network test for neglected nonlinearity. Econom. J. 6 (2), 357–373.
Butler, L., West, J.S., Tighe, S.L., 2013. Effect of recycled concrete coarse aggregate from multiple sources on the hardened properties of concrete with equivalent compressive strength. Constr. Build. Mater. 47, 1292–1301.
Butler, L.J., West, J.S., Tighe, S.L., 2014. Towards the classification of recycled concrete aggregates: influence of fundamental aggregate properties on recycled concrete performance. J. Sustain. Cem.-Based Mater. 3 (2), 140–163.
Çakır, Ö., Sofyanlı, Ö.Ö., 2015. Influence of silica fume on mechanical and physical properties of recycled aggregate concrete. HBRC J. 11 (2), 157–166.
Carneiro, J.A., Lima, P.R.L., Leite, M.B., Toledo Filho, R.D., 2014. Compressive stress–strain behavior of steel fiber reinforced-recycled aggregate concrete. Cem. Concr. Compos. 46, 65–72.
Casuccio, M., Torrijos, M., Giaccio, G., Zerbino, R., 2008. Failure mechanism of recycled aggregate concrete. Constr. Build. Mater. 22 (7), 1500–1506.
Chaabene, W.B., Flah, M., Nehdi, M.L., 2020. Machine learning prediction of mechanical properties of concrete: critical review. Constr. Build. Mater. 260, 119889.
Chen, H., Qi, G., Yang, J., Amini, F., 1995. Neural network for structural dynamic model identification. J. Eng. Mech. 121 (12), 1377–1381.
Chen, S.-.C., Lin, W.-.T., Huang, R., Hsu, H.-.M., 2021. Performance of green concrete and inorganic coating materials. Materials (Basel) 14 (4), 832.
Cook, R., Lapeyre, J., Ma, H., Kumar, A., 2019. Prediction of compressive strength of concrete: critical comparison of performance of a hybrid machine learning model with standalone models. J. Mater. Civ. Eng. 31 (11), 04019255.
Corinaldesi, V., 2010. Mechanical and elastic behaviour of concretes made of recycled-concrete coarse aggregates. Constr. Build. Mater. 24 (9), 1616–1620.
Deng, S., Zhou, X., Huang, A., Yih, Y., Sutherland, J.W., 2021. Evaluating economic opportunities for product recycling via the Sherwood principle and machine learning. Resour. Conserv. Recycl. 167, 105232.
Dhanya, B., Koshy, B.I., Jisha, K., Jayamohanan, A., Mathew, N., 2020. Evaluation of the mechanical performance of M25 grade recycled aggregate concrete. In: IOP Conference Series: Earth and Environmental Science. IOP Publishing, 012034.
Dilbas, H., Güneş, M.Ş., 2021. Mineral addition and mixing methods effect on recycled aggregate concrete. Materials (Basel) 14 (4), 907.
Dilbas, H., Şimşek, M., Çakır, Ö., 2014. An investigation on mechanical and physical properties of recycled aggregate concrete (RAC) with and without silica fume. Constr. Build. Mater. 61, 50–59.
Domingo-Cabo, A., Lázaro, C., López-Gayarre, F., Serrano-López, M., Serna, P., Castaño-Tabares, J.O., 2009. Creep and shrinkage of recycled aggregate concrete. Constr. Build. Mater. 23 (7), 2545–2553.
Du, Y., Zhao, Z., Xiao, Q., Shi, F., Yang, J., Gao, P., 2021. Experimental study on the mechanical properties and compression size effect of recycled aggregate concrete. Materials (Basel) 14 (9), 2323.
Duan, Z., Singh, A., Xiao, J., Hou, S., 2020. Combined use of recycled powder and recycled coarse aggregate derived from construction and demolition waste in self-compacting concrete. Constr. Build. Mater. 254, 119323.
Duan, Z.H., Poon, C.S., 2014. Properties of recycled aggregate concrete made with recycled aggregates with different amounts of old adhered mortars. Mater. Des. 58, 19–29.
Etxeberria, M., Marí, A.R., Vázquez, E., 2007a. Recycled aggregate concrete as structural material. Mater. Struct. 40 (5), 529–541.
Etxeberria, M., Vázquez, E., Marí, A., Barra, M., 2007b. Influence of amount of recycled coarse aggregates and production process on properties of recycled aggregate concrete. Cem. Concr. Res. 37 (5), 735–742.
Fathifazl, G., Razaqpur, A.G., Isgor, O.B., Abbas, A., Fournier, B., Foo, S., 2011. Creep and drying shrinkage characteristics of concrete produced with coarse recycled concrete aggregate. Cem. Concr. Compos. 33 (10), 1026–1037.
Fiol, F., Thomas, C., Manso, J., López, I., 2020. Influence of recycled precast concrete aggregate on durability of concrete's physical processes. Appl. Sci. 10 (20), 7348.
Folino, P., Xargay, H., 2014. Recycled aggregate concrete–mechanical behavior under uniaxial and triaxial compression. Constr. Build. Mater. 56, 21–31.
Friedman, J.H., 2001. Greedy function approximation: a gradient boosting machine. Ann. Stat. 1189–1232.
Gao, D., Zhang, L., Nokken, M., Zhao, J., 2019. Mixture proportion design method of steel fiber reinforced recycled coarse aggregate concrete. Materials (Basel) 12 (3), 375.

Gao, H., Wu, G., Yuan, X., 2015. Experimental research on mechanical properties of recycled aggregate concrete with different modification methods. In: 3rd International Conference on Material, Mechanical and Manufacturing Engineering (IC3ME 2015). Atlantis Press, pp. 1957–1962.
García-González, J., Rodríguez-Robles, D., Juan-Valdés, A., Morán-del Pozo, J.M., Guerra-Romero, M.I., 2015. Porosity and pore size distribution in recycled concrete. Mag. Concr. Res. 67 (22), 1214–1221.
Gayarre, F.L., Perez, C.L.C., Lopez, M.A.S., Cabo, A.D., 2014. The effect of curing conditions on the compressive strength of recycled aggregate concrete. Constr. Build. Mater. 53, 260–266.
Gökçe, H.S., Şimşek, O., 2013. The effects of waste concrete properties on recycled aggregate concrete properties. Mag. Concr. Res. 65 (14), 844–854.
Gómez-Soberón, J.M., 2002. Porosity of recycled concrete with substitution of recycled concrete aggregate: an experimental study. Cem. Concr. Res. 32 (8), 1301–1311.
Gomez, J., Agullo, L., Vazquez, E., 2001. Relationship between porosity and concrete properties with natural aggregate replacement by recycled concrete aggregate. In: Second International Conference on Engineering Materials, pp. 147–156.
Gonzalez-Corominas, A., Etxeberria, M., 2016. Effects of using recycled concrete aggregates on the shrinkage of high performance concrete. Constr. Build. Mater. 115, 32–41.
González-Fonteboa, B., Martínez-Abella, F., 2008. Concretes with aggregates from demolition waste and silica fume. Materials and mechanical properties. Build. Environ. 43 (4), 429–437.
González, M.D., Plaza Caballero, P., Fernández, D.B., Jordán Vidal, M.M., Del Bosque, I. F.S., Medina Martínez, C., 2021. The design and development of recycled concretes in a circular economy using mixed construction and demolition waste. Materials (Basel) 14 (16), 4762.
Gunasekara, C., Seneviratne, C., Law, D.W., Setunge, S., 2020. Feasibility of developing sustainable concrete using environmentally friendly coarse aggregate. Appl. Sci. 10 (15), 5207.
Guo, H., Shi, C.J., Guan, X.M., Zhu, J.P., Ding, Y.H., Ling, T.C., Zhang, H.B., Wang, Y.L., 2018. Durability of recycled aggregate concrete - a review. Cem. Concr. Compos. 89, 251–259.
Guo, J., Chen, Q., Chen, W., Cai, J., 2019. Tests and numerical studies on strain-rate effect on compressive strength of recycled aggregate concrete. J. Mater. Civ. Eng. 31 (11), 04019281.
Gupta, P.K., Rajhans, P., Panda, S., Nayak, S., Das, S.K., 2020. Mix design method for self-compacting recycled aggregate concrete and its microstructural investigation by considering adhered mortar in aggregate. J. Mater. Civ. Eng. 32 (3), 04019371.
Habibi, A., Ramezanianpour, A.M., Mahdikhani, M., 2021. RSM-based optimized mix design of recycled aggregate concrete containing supplementary cementitious materials based on waste generation and global warming potential. Resour. Conserv. Recycl. 167, 105420.
Haitao, Y., Shizhu, T., 2015. Preparation and properties of high-strength recycled concrete in cold areas. Mater. Constr. 65 (318) e050-e050.
Her, S., Park, T., Zalnezhad, E., Bae, S., 2021. Synthesis and characterization of cement clinker using recycled pulverized oyster and scallop shell as limestone substitutes. J. Clean. Prod. 278.
Huang, Q., Lin, L., Tan, E.L., Singh, B., 2017. Mix design of recycled aggregate concrete using packing density method. In: Proc. 1st Int. Conf. Struct. Eng. Res, pp. 20–22.
Ismail, S., Ramli, M., 2013. Engineering properties of treated recycled concrete aggregate (RCA) for structural applications. Constr. Build. Mater. 44, 464–476.
Jo, J.-.M., 2019. Effectiveness of normalization pre-processing of big data to the machine learning performance. J. Korea Inst. Electron. Commun. Sci. 14 (3), 547–552.
Juan-Valdes, A., Rodriguez-Robles, D., Garcia-Gonzalez, J., de Rojas Gómez, M.I.S., Guerra-Romero, M.I., De Belie, N., Morán-del Pozo, J.M., 2021. Mechanical and microstructural properties of recycled concretes mixed with ceramic recycled cement and secondary recycled aggregates. A viable option for future concrete. Constr. Build. Mater. 270, 121455.
Kannan, S., Arunachalam, K., Brindha, D., 2021. Performance analysis of recycled aggregate concrete with chemical admixture. Struct. Concrete 22, E8–E21.
Kazmi, S.M.S., Munir, M.J., Wu, Y.-.F., 2021. Application of waste tire rubber and recycled aggregates in concrete products: a new compression casting approach. Resour. Conserv. Recycl. 167, 105353.
Kim, K., Shin, M., Cha, S., 2013. Combined effects of recycled aggregate and fly ash towards concrete sustainability. Constr. Build. Mater. 48, 499–507.
Kim, N., Kim, J., Yang, S., 2016. Mechanical strength properties of RCA concrete made by a modified EMV method. Sustainability 8 (9), 924.
Kim, S.-.W., Yun, H.-.D., Park, W.-.S., Jang, Y.-.I., 2015. Bond strength prediction for deformed steel rebar embedded in recycled coarse aggregate concrete. Mater. Des. 83, 257–269.
Kim, Y., Hanif, A., Usman, M., Park, W., 2019. Influence of bonded mortar of recycled concrete aggregates on interfacial characteristics–porosity assessment based on pore segmentation from backscattered electron image analysis. Constr. Build. Mater. 212, 149–163.
Kou, S.-c., Poon, C.-s., Agrela, F., 2011a. Comparisons of natural and recycled aggregate concretes prepared with the addition of different mineral admixtures. Cem. Concr. Compos. 33 (8), 788–795.
Kou, S.-.C., Poon, C.-.S., Etxeberria, M., 2011b. Influence of recycled aggregates on long term mechanical properties and pore size distribution of concrete. Cem. Concr. Compos. 33 (2), 286–291.
Kou, S.C., Poon, C.S., Etxeberria, M., 2014. Residue strength, water absorption and pore size distributions of recycled aggregate concrete after exposure to elevated temperatures. Cem. Concr. Compos. 53, 73–82.
Kwan, W.H., Ramli, M., Kam, K.J., Sulieman, M.Z., 2012. Influence of the amount of recycled coarse aggregate in concrete design and durability properties. Constr. Build. Mater. 26 (1), 565–573.
Lera, G., Pinzolas, M., 2002. Neighborhood based Levenberg-Marquardt algorithm for neural network training. IEEE Trans. Neural Netw. 13 (5), 1200–1203.
Li, C., Liu, T., Fu, H., Zhang, X., Yang, Y., Zhao, S., 2021. Test and evaluation of the flexural properties of reinforced concrete beams with 100% recycled coarse aggregate and manufactured sand. Buildings 11 (9), 420.
Liang, J.-.F., Yang, Z.-.P., Yi, P.-.H., Wang, J.-.B., 2017. Stress-strain relationship for recycled aggregate concrete after exposure to elevated temperatures. Comput. Concr. 19 (6), 609–615.
Liang, M., Chang, Z., Wan, Z., Gan, Y., Schlangen, E., Šavija, B., 2021a. Interpretable ensemble-machine-learning models for predicting creep behavior of concrete. Cem. Concr. Compos. 125, 104295.
Liang, X., Yan, F., Chen, Y., Wu, H., Ye, P., Mo, Y., 2021b. Study on the strength performance of recycled aggregate concrete with different ages under direct shearing. Materials (Basel) 14 (9), 2312.
Lin, Y.-.H., Tyan, Y.-.Y., Chang, T.-.P., Chang, C.-.Y., 2004. An assessment of optimal mixture for concrete made with recycled concrete aggregates. Cem. Concr. Res. 34 (8), 1373–1380.
Ling, L., Jiguang, C., 2018. Effect of concretion wastes recycled aggregate on concrete performance.
Liu, J., Ren, F., Quan, H., 2021. Prediction model for compressive strength of porous concrete with low-grade recycled aggregate. Materials (Basel) 14 (14), 3871.
Ma, M.X., Tam, V.W.Y., Le, K.N., Osei-Kyei, R., 2022. Factors affecting the price of recycled concrete: a critical review. J. Build. Eng. 46.
Malešev, M., Radonjanin, V., Marinković, S., 2010. Recycled concrete as aggregate for structural concrete production. Sustainability 2 (5), 1204–1225.
Manzi, S., Mazzotti, C., Bignozzi, M.C., 2013. Short and long-term behavior of structural concrete with recycled concrete aggregate. Cem. Concr. Compos. 37, 312–318.
Manzi, S., Mazzotti, C., Bignozzi, M.C., 2017. Self-compacting concrete with recycled concrete aggregate: study of the long-term properties. Constr. Build. Mater. 157, 582–590.
Martinez, C.M., del Bosque, I.S., Medina, G., Frías, M., de Rojas, M.S., 2022. Thermal performance of concrete with recycled concrete powder as partial cement replacement and recycled CDW aggregate. The Structural Integrity of Recycled Aggregate Concrete Produced with Fillers and Pozzolans, pp. 105–143.
Medina, C., Zhu, W., Howind, T., de Rojas, M.I.S., Frías, M., 2014. Influence of mixed recycled aggregate on the physical–mechanical properties of recycled concrete. J. Clean. Prod. 68, 216–225.
Mohammed, N., Sarsam, K., Hussien, M., 2018. The influence of recycled concrete aggregate on the properties of concrete. In: MATEC Web of Conferences. EDP Sciences, p. 02020.
Molnar, C., Freiesleben, T., König, G., Casalicchio, G., Wright, M.N., Bischl, B., 2021. Relating the partial dependence plot and permutation feature importance to the data generating process. arXiv preprint arXiv:2109.01433.
Nepomuceno, M.C., Isidoro, R.A., Catarino, J.P., 2018. Mechanical performance evaluation of concrete made with recycled ceramic coarse aggregates from industrial brick waste. Constr. Build. Mater. 165, 284–294.
Nieto, D., Dapena, E., Alaejos, P., Olmedo, J., Pérez, D., 2019. Properties of self-compacting concrete prepared with coarse recycled concrete aggregates and different water: cement ratios. J. Mater. Civ. Eng. 31 (2), 04018376.
Nili, M., Sasanipour, H., Aslani, F., 2019. The effect of fine and coarse recycled aggregates on fresh and mechanical properties of self-compacting concrete. Materials (Basel) 12 (7), 1120.
Nunes, K.R.A., Mahler, C.F., 2020. Comparison of construction and demolition waste management between Brazil, European Union and USA. Waste Manag. Res. 38 (4), 415–422.
Ozbakkaloglu, T., Gholampour, A., Xie, T., 2018. Mechanical and durability properties of recycled aggregate concrete: effect of recycled aggregate properties and content. J. Mater. Civ. Eng. 30 (2), 04017275.
Pani, L., Francesconi, L., Rombi, J., Mistretta, F., Sassu, M., Stochino, F., 2020. Effect of parent concrete on the performance of recycled aggregate concrete. Sustainability 12 (22), 9399.
Pavlů, T., Kočí, V., Hajek, P., 2019. Environmental assessment of two use cycles of recycled aggregate concrete. Sustainability 11 (21), 6185.
Peng, J.-.L., Du, T., Zhao, T.-.S., Song, X.-q., Tang, J.-.J., 2019. Stress–strain relationship model of recycled concrete based on strength and replacement rate of recycled coarse aggregate. J. Mater. Civ. Eng. 31 (9), 04019189.
Peng, Y., Unluer, C., 2022. Analyzing the mechanical performance of fly ash-based geopolymer concrete with different machine learning techniques. Constr. Build. Mater. 316, 125785.
Pereira-de-Oliveira, L., Nepomuceno, M., Castro-Gomes, J., Vila, M.d.F.C., 2014. Permeability properties of self-compacting concrete with coarse recycled aggregates. Constr. Build. Mater. 51, 113–120.
Poon, C.S., Kou, S., Lam, L., 2007. Influence of recycled aggregate on slump and bleeding of fresh concrete. Mater. Struct. 40 (9), 981–988.
Poon, C.S., Shui, Z., Lam, L., 2004a. Effect of microstructure of ITZ on compressive strength of concrete prepared with recycled aggregates. Constr. Build. Mater. 18 (6), 461–468.
Poon, C.S., Shui, Z., Lam, L., Fok, H., Kou, S., 2004b. Influence of moisture states of natural and recycled aggregates on the slump and compressive strength of concrete. Cem. Concr. Res. 34 (1), 31–36.
Poudyal, L., Adhikari, K., 2021. Environmental sustainability in cement industry: an integrated approach for green and economical cement production. Resour. Environ. Sustain. 4, 100024.

Qi, C., Fourie, A., Chen, Q., 2018. Neural network and particle swarm optimization for predicting the unconfined compressive strength of cemented paste backfill. Constr. Build. Mater. 159, 473–478.
Rangel, C.S., Amario, M., Pepe, M., Martinelli, E., Toledo Filho, R.D., 2020. Influence of wetting and drying cycles on physical and mechanical behavior of recycled aggregate concrete. Materials (Basel) 13 (24), 5675.
Rosa, L., Becattini, V., Gabrielli, P., Andreotti, A., Mazzotti, M., 2022. Carbon dioxide mineralization in recycled concrete aggregates can contribute immediately to carbon-neutrality. Resour. Conserv. Recycl. 184, 106436.
Saha, P., Debnath, P., Thomas, P., 2020. Prediction of fresh and hardened properties of self-compacting concrete using support vector regression approach. Neural Comput. Appl. 32 (12), 7995–8010.
Santos, S.A., Da Silva, P.R., De Brito, J., 2017. Mechanical performance evaluation of self-compacting concrete with fine and coarse recycled aggregates from the precast industry. Materials (Basel) 10 (8), 904.
Savva, P., Ioannou, S., Oikonomopoulou, K., Nicolaides, D., Petrou, M.F., 2021. A mechanical treatment method for recycled aggregates and its effect on recycled aggregate-based concrete. Materials (Basel) 14 (9), 2186.
Setkit, M., Leelatanon, S., Imjai, T., Garcia, R., Limkatanyu, S., 2021. Prediction of shear strength of reinforced recycled aggregate concrete beams without stirrups. Buildings 11 (9), 402.
Sharaky, I., Issa, U., Alwetaishi, M., Abdelhafiz, A., Shamseldin, A., Al-Surf, M., Al-Harthi, M., Balabel, A., 2021. Strength and water absorption of sustainable concrete produced with recycled basaltic concrete aggregates and powder. Sustainability 13 (11), 6277.
Sheen, Y.-.N., Wang, H.-.Y., Juang, Y.-.P., Le, D.-.H., 2013. Assessment on the engineering properties of ready-mixed concrete using recycled aggregates. Constr. Build. Mater. 45, 298–305.
Shi, C.J., Li, Y.K., Zhang, J.K., Li, W.G., Chong, L.L., Xie, Z.B., 2016. Performance enhancement of recycled concrete aggregate - a review. J. Clean. Prod. 112, 466–472.
Silva, F.A., Delgado, J.M., Azevedo, A.C., Lima, A.G., Vieira, C.S., 2021. Preliminary analysis of the use of construction waste to replace conventional aggregates in concrete. Buildings 11 (3), 81.
Soares, D., De Brito, J., Ferreira, J., Pacheco, J., 2014. Use of coarse recycled aggregates from precast concrete rejects: mechanical and durability performance. Constr. Build. Mater. 71, 263–272.
Somna, R., Jaturapitakkul, C., Chalee, W., Rattanachu, P., 2012. Effect of the water to binder ratio and ground fly ash on properties of recycled aggregate concrete. J. Mater. Civ. Eng. 24 (1), 16–22.
Sriravindrarajah, R., Wang, N.D.H., Ervin, L.J.W., 2012. Mix design for pervious recycled aggregate concrete. Int. J. Concr. Struct. Mater. 6 (4), 239–246.
Taffese, W.Z., 2018. Suitability investigation of recycled concrete aggregates for concrete production: an experimental case study. Adv. Civ. Eng. 2018.
Tam, V.W., Butera, A., Le, K.N., Li, W., 2020. Utilising CO2 technologies for recycled aggregate concrete: a critical review. Constr. Build. Mater. 250, 118903.
Tam, V.W., Kotrayothar, D., Xiao, J., 2015. Long-term deformation behaviour of recycled aggregate concrete. Constr. Build. Mater. 100, 262–272.
Tam, V.W.Y., Soomro, M., Evangelista, A.C.J., Haddad, A., 2021. Deformation and permeability of recycled aggregate concrete - a comprehensive review. J. Build. Eng. 44.
Tang, W., Ryan, P., Cui, H., Liao, W., 2016. Properties of self-compacting concrete with recycled coarse aggregate. Adv. Mater. Sci. Eng. 2016.
Thomas, C., Setién, J., Polanco, J., Cimentada, A., Medina, C., 2018. Influence of curing conditions on recycled aggregate concrete. Constr. Build. Mater. 172, 618–625.
Ulloa, V.A., García-Taengua, E., Pelufo, M.-.J., Domingo, A., Serna, P., 2013. New views on effect of recycled aggregates on concrete compressive strength. ACI Mater. J. 110 (6), 1–10.
Wang, B., Yan, L., Fu, Q., Kasal, B., 2021. A comprehensive review on recycled aggregate and recycled aggregate concrete. Resour. Conserv. Recycl. 171, 105565.
Winter, E., 2002. The Shapley value. Handbook of Game Theory with Economic Applications 3, 2025–2054.
Xiao, J.Z., Li, W.G., Sun, Z.H., Lange, D.A., Shah, S.P., 2013. Properties of interfacial transition zones in recycled aggregate concrete tested by nanoindentation. Cem. Concr. Compos. 37, 276–292.
Yan, K., Shi, C., 2010. Prediction of elastic modulus of normal and high strength concrete by support vector machine. Constr. Build. Mater. 24 (8), 1479–1485.
Yang, K.-.H., Chung, H.-.S., Ashour, A.F., 2008. Influence of type and replacement level of recycled aggregates on concrete properties.
Yang, S., 2018. Effect of different types of recycled concrete aggregates on equivalent concrete strength and drying shrinkage properties. Appl. Sci. 8 (11), 2190.
Yeh, I.-.C., 1998. Modeling of strength of high-performance concrete using artificial neural networks. Cem. Concr. Res. 28 (12), 1797–1808.
Younis, K.H., Pilakoutas, K., 2013. Strength prediction model and methods for improving recycled aggregate concrete. Constr. Build. Mater. 49, 688–701.
Yuan, Z., Wang, L.-.N., Ji, X., 2014. Prediction of concrete compressive strength: research on hybrid models genetic based algorithms and ANFIS. Adv. Eng. Softw. 67, 156–163.
Zhang, J., Huang, Y., Ma, G., Nener, B., 2021. Mixture optimization for environmental, economical and mechanical objectives in silica fume concrete: a novel frame-work based on machine learning and a new meta-heuristic algorithm. Resour. Conserv. Recycl. 167, 105395.